International Journal of Thermophysics, Vol. 23, No. 2, March 2002 (© 2002)

Noncontact Measurements of Thermophysical Properties of Molybdenum at High Temperatures

P.-F. Paradis,[1, 2] T. Ishikawa,[1] and S. Yoda[1]

Received July 6, 2001

Four thermophysical properties of both solid and liquid molybdenum, namely, the density, the thermal expansion coefficient, the constant-pressure heat capacity, and the hemispherical total emissivity, are reported. These thermophysical properties were measured over a wide temperature range, including the undercooled state, using an electrostatic levitation furnace developed by the National Space Development Agency of Japan. Over the 2500 to 3000 K temperature span, the density of the liquid can be expressed as $\rho_L(T) = 9.10 \times 10^3 - 0.60(T - T_m)$ $(kg \cdot m^{-3})$, with $T_m = 2896$ K, yielding a volume expansion coefficient $\alpha_L(T) = 6.6 \times 10^{-5}$ (K^{-1}). Similarly, over the 2170 to 2890 K temperature range, the density of the solid can be expressed as $\rho_S(T) = 9.49 \times 10^3 - 0.50(T - T_m)$, giving a volume expansion coefficient $\alpha_S(T) = 5.3 \times 10^{-5}$. The constant pressure heat capacity of the liquid phase could be estimated as $C_{PL}(T) = 34.2 + 1.13 \times 10^{-3}(T - T_m)$ $(J \cdot mol^{-1} \cdot K^{-1})$ if the hemispherical total emissivity of the liquid phase remained constant at 0.21 over the temperature interval. Over the 2050 to 2890 K temperature span, the hemispherical total emissivity of the solid phase could be expressed as $\varepsilon_{TS}(T) = 0.29 + 9.86 \times 10^{-5}(T - T_m)$. The latent heat of fusion has also been measured as 33.6 $kJ \cdot mol^{-1}$.

KEY WORDS: density; hemispherical total emissivity; latent heat of fusion; liquid metal; molten molybdenum; noncontact processing.

1. INTRODUCTION

Due to its refractory nature and resistance to corrosion, molybdenum has been employed primarily to harden alloys used by the aerospace industry and in nuclear reactors. Molybdenum has also found applications as filament material in electronic and electrical devices [1]. However, its high

[1] National Space Development Agency of Japan, Tsukuba Space Center, 2-1-1 Sengen, Tsukuba City, Ibaraki 305-8505, Japan.
[2] To whom correspondence should be addressed. E-mail: paradis.paulfrancois@nasda.go.jp

0195-928X/02/0300-0555/0 © 2002 Plenum Publishing Corporation

melting temperature (2896 K) and the risk of contamination at elevated temperature [1] make it difficult to measure the thermophysical properties of its solid phase at high temperatures and even more problematic for those of its superheated and undercooled phases using traditional methods. This motivated the use of containerless methods and noncontact diagnostic techniques. The electrostatic levitation furnace (ELF) developed by the National Space Development Agency of Japan (NASDA) circumvented the difficulties associated with high-temperature processing and allowed accurate and quick determination of the thermophysical properties of different materials [2–9]. High-temperature processing was achieved in vacuum by using multiple laser heating beams, thus isolating the sample from contaminating walls as well as surrounding gases and providing sufficient stability for the thermophysical properties to be measured. The facility also permitted deep undercooling of the levitated sample which was not heated by the electrostatic scheme and because of containerless conditions and fast radiative cooling. Also, since the sample was free from any enclosure, it represented an easy target for various diagnostic detectors and probes.

Besides its use for thermophysical properties determination, this facility has a wide range of potential applications. For example, it can be used to synthesize new materials, in particular, glass-forming materials and alloys, with novel properties. Although its best feature lies in its ability to handle corrosive liquids, it is also attractive for the study of certain solids, such as niobium and molybdenum, that exhibit a corrosive activity at high temperatures. A similar facility, currently under development by NASDA, will be dedicated to the analysis of the atomic structure of overheated and undercooled materials by neutron scattering experiments.

An accurate knowledge of thermophysical properties is paramount for various fundamental studies on nucleation and phase transformations, as well as industrial processes on metals, such as casting, refining, and forming. Moreover, the properties can sometimes be used to determine other thermophysical quantities. For example, enthalpy, entropy, and Gibbs free energy can be derived from the heat capacity. The present paper focuses on the thermophysical properties of high-temperature solid and liquid molybdenum, namely, density, thermal expansion coefficient, constant-pressure heat capacity, and hemispherical total emissivity. The value of the latent heat of fusion was also calculated from the data.

2. EXPERIMENTAL SETUP AND PROCEDURES

2.1. Electrostatic Levitation Furnace

The measurements reported in this paper were carried out using an electrostatic levitation furnace developed by NASDA [3–7]. The apparatus

was based on a design by Rhim et al. [10] with modifications in the areas of sample levitation initiation, charging, handling, imaging, and heating configuration without which the described experiments would have been difficult to perform [6]. Figure 1a illustrates the electrostatic levitation furnace schematically. The facility consists of a stainless-steel chamber which was evacuated to $\sim 10^{-5}$ Pa before the sample processing was initiated. The chamber housed the sample that was levitated between two parallel disk electrodes, typically 10 mm apart. These electrodes were used for vertical position sample control (Fig. 1b). In addition, four spherical electrodes distributed around the bottom electrode were used for horizontal position control via a feedback loop. The lower electrode was also surrounded by four coils that generated a rotating magnetic field which was used for rotation control [11]. The top electrode was gimbaled by four micrometer screws, allowing electrode balancing and separation control. The bottom electrode had a central hole that permitted sample handling. A cartridge, with a 10-sample capacity, contained individual molybdenum pedestals, thus eliminating any contamination problems. For these experiments, specimens were prepared by arc-melting 3N5 molybdenum wire (Nilaco

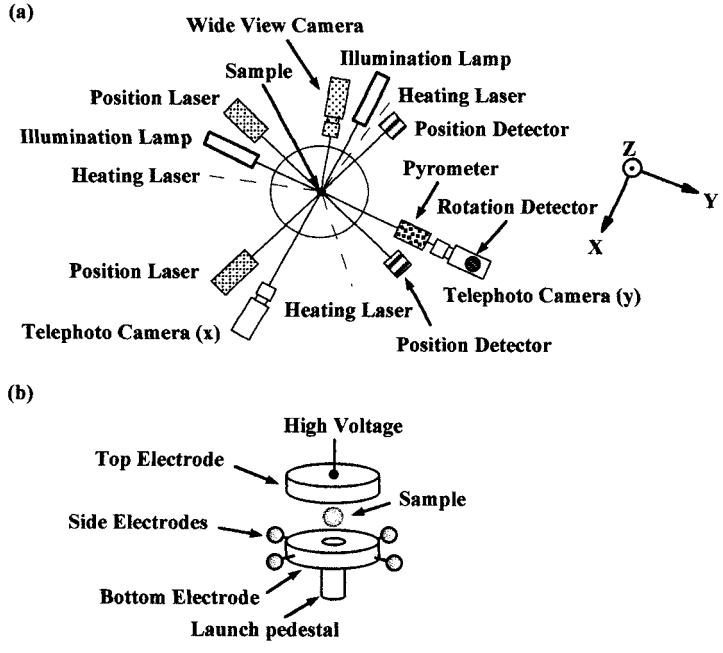

Fig. 1. Schematic view of NASDA's electrostatic levitation furnace (a) and electrode assembly (b).

Corporation, Tokyo) into spheroids with diameter of ca. 1.5 mm. A conical catcher was used to retrieve an unsuccessfully levitated sample. The positioning system used a set of orthogonally disposed He–Ne lasers and the associated position detectors. The sample position information was fed to a computer that input new values of x, y, and z to high-voltage amplifiers at a rate of nearly 720 Hz (z direction) so that a prefixed position could be maintained.

Sample heating was performed using two 100-W CO_2 lasers (Synrad, Evolution 100) emitting at 10.6 μm. One beam was sent directly to the sample, whereas the other beam was divided into two portions such that three focused beams, separated by 120°, hit the specimen. Accurate computer control ensured that each beam delivered equal power to the sample. The control software also allowed quick radiative cooling by simply turning off the laser power. The heating configuration, together with controlled low-frequency sample rotation ($\ll 10$ Hz), ensured good temperature homogeneity. Temperature data were obtained over a 1070-to-3800 K temperature interval using two commercially available automatic pyrometers (Chino Corp. Model IR-CS 2S CG, operating at 0.90 μm, and Chino Corp. Model IR-AP, operating at 0.96 μm) with respective acquisition rates of 10 and 120 Hz. Due to the high evaporation rate of molybdenum, particular care was taken to maintain clean view ports, in particular, that of the pyrometer. Previous experiments with tin samples showed that patches of oxides floating on a liquid sample could be easily detected visually either with telephoto cameras or with our He–Ne laser-based sample rotation detection system. Traces of oxidation were observed on solid molybdenum prior to melting. However, these unstable oxides were easy to break, disappeared, and were tracked neither by the rotation detection nor by visual observation when the sample was liquefied. Even when the sample solidified, the recurrence of oxide patches was not observed.

The sample was observed by three charged-coupled-device (CCD) cameras (Fig. 1a). One camera offered a general view of both the electrode assembly and the sample. Another camera looked along the same path as a pyrometer to ensure its constant alignment, to monitor the sample position in the horizontal plane, and to align the heating laser beams to minimize any detrimental photon pressure effects such as rotation and oscillation on the levitated sample [12]. Sample imaging for thermophysical properties determination was achieved by a high-resolution, black-and-white CCD videocamera (Sony SSC-M370) equipped with a telephoto objective and a high-pass filter (450 nm), in conjunction with a high-intensity ultraviolet background light. This gave a close look at the sample, allowing perimeter and surface features to be analyzed. The use of the ultraviolet lamp and the filter gave a background lighting efficiency that was practically independent

of the sample temperature (from an overheated liquid to a room-temperature sample), yielding excellent imaging, thus allowing accurate determination of both the density and the ratio of the constant-pressure heat capacity and the hemispherical total emissivity. Details about this technique can be found elsewhere [6].

Although processing metals with low melting temperatures (Sn, NiZr, etc.) had not posed any particular difficulties when the current electrostatic levitation furnaces were used [10, 13], the time required to bring a sample into a state at which its thermophysical properties can be measured can sometimes last for several hours depending on the material [14]. Because the lengthy processing time limited the number of experiments and posed some constraints in terms of sample evaporation and electrode coating (affects levitation), it was detrimental when measuring the thermophysical properties. In the new levitation initiation method implemented by NASDA [6], the sample, in its launching position on the pedestal, was heated while monitoring its temperature with a pyrometer. The sample was heated with one beam, whereas the two remaining beams converged at the location at which the sample was going to be positioned after the launch. Once the sample reached a temperature close to 1500 K, at which the thermionic emission was sufficient to charge the sample; the high voltage between the two electrodes was applied, and the feedback control software was activated. A few seconds later, the sample was launched into its normal levitation position. When the hot sample was levitated, the preheating laser beam was redirected on the sample.

2.2. Thermophysical Properties Determination

Density and the quotient of constant pressure heat capacity (C_p) and hemispherical total emissivity (ε_T) were measured using the vacuum version of the NASDA-ELF. Details of these techniques have been described in the literature and are summarized below [15, 16].

The measurements were taken after a spheroid sample was first molten and resolidified. This ensured that the pyrometer was correctly calibrated and aligned and that the sample, prepared by arc-melting, became truly spherical. In case the shape of a liquefied sample departed from a sphere (due to rotation), a counter torque was applied either with a magnetic field [11] or by appropriately steering the beams of the heating lasers [12] to restore the spherical shape. Hence, the measurements were taken only on spherical samples, whether they were in their solid or liquid phases. Once the sample was molten, as illustrated for molybdenum (Fig. 2), it took a spherical shape due to surface tension and the distribution of surface charge. Also, since the electrostatic scheme did not input any heat, a heated

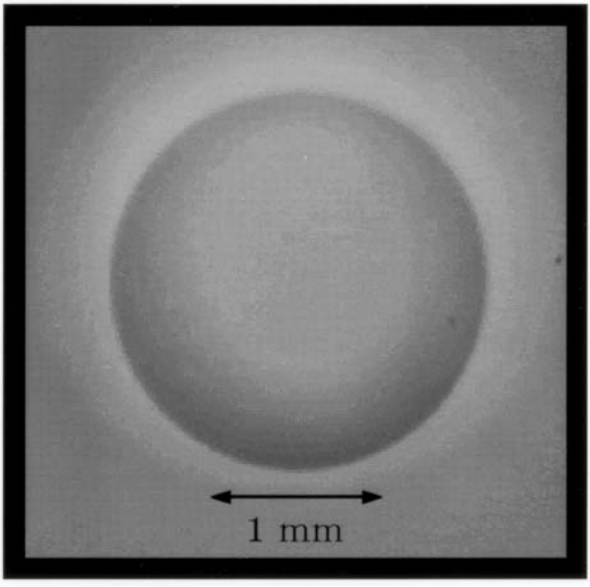

Fig. 2. Side view of a levitated molten molybdenum sample.

sample experienced pure radiative cooling when heating laser beams were blocked. The resulting energy equation governing the cooling process is given as

$$(mC_p/M)\, dT/dt = \varepsilon_T A\sigma(T^4 - T_{amb}^4) \tag{1}$$

where m is the sample mass, M is the molar mass, C_p is the constant pressure molar heat capacity, ε_T is the hemispherical total emissivity, A is the sample area, σ is the Stefan–Boltzmann constant, and T and T_{amb} are, respectively, the sample and ambient temperatures. The radiance temperature was measured by the pyrometers and was calibrated to true temperature using the known melting temperature of the sample ($T_m = 2896$ K). Calibration to true temperature was performed using a custom-made Code Warrior software. A typical cooling curve for molybdenum showing a 450 K undercooling and the recalescence (sudden temperature rise due to the release of the latent heat of fusion of an undercooled sample upon solidification) is shown in Fig. 3. Because the sample was heated to a temperature of only 100 K above the melting point, the cooling rates of the liquid and that of the solid (over a similar temperature range) were very similar. However, the radiative cooling rate having a dependence with the fourth power of the temperature, the cooling rate of the solid at

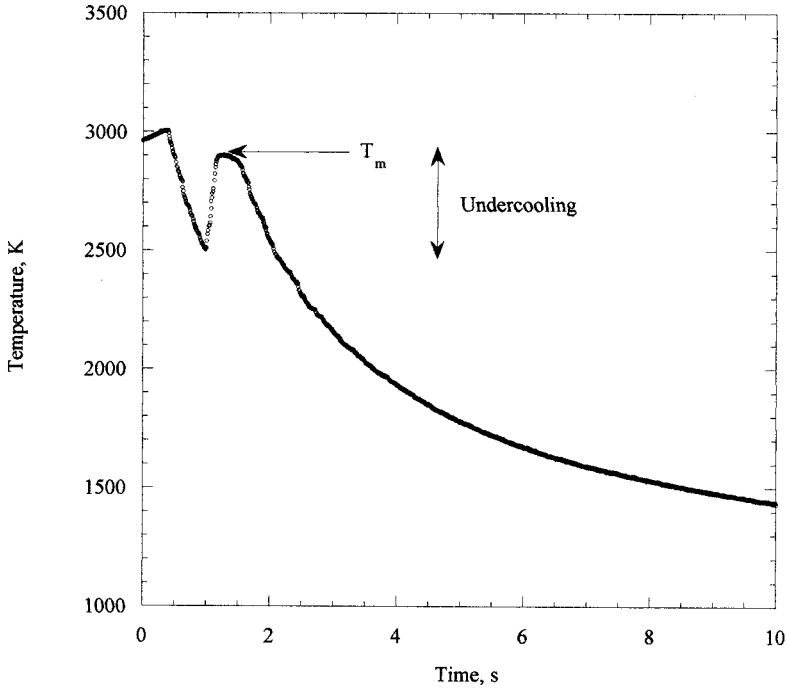

Fig. 3. Radiative cooling curve for molybdenum showing undercooling and recalescence.

temperatures, say, below the lowest level of undercooling, decreased substantially. The undercooling level achieved was, within the experimental errors, similar to that obtained by Hofmeister et al. [17] with a drop tube and in agreement with the classical nucleation theory proposed by Turnbull [18]. After the sample started to cool, both the image and the cooling curve data could be used to measure simultaneously the density and the ratio of constant-pressure heat capacity and hemispherical total emissivity. For density measurements, the recorded video images (Fig. 2) were digitized and matched to the cooling curve. Then NASDA developed software extracted the area from each image. Since the sample was axisymmetric and because its mass was known, the density could be found for each temperature.

The ratio of constant-pressure heat capacity and hemispherical total emissivity could be found from Eq. (1) since all parameters were known, and since the area was found from the images and dT/dt from the cooling curve.

3. EXPERIMENTAL RESULTS

3.1. Density

The results of our density measurements for liquid molybdenum are shown in Fig. 4. The measurements were taken over the 2500 to 3000 K temperature range and covered the undercooled region by nearly 400 K. The density of liquid molybdenum, as that of other pure metals, exhibited a linear behavior as a function of temperature and could be fitted by the following equation:

$$\rho_L(T) = 9.10 \times 10^3 - 0.60(T - T_m)\ (\mathrm{kg \cdot m^{-3}}) \qquad (2500\ \text{to}\ 3000\ \mathrm{K}) \qquad (2)$$

where T_m is the melting temperature (2896 K). In this experiment, the uncertainty of the measurements was estimated to be less than 2% from the resolution of the video grabbing capabilities (640×480 pixels) and from the uncertainty in mass measurement (± 0.0001 g). To our knowledge, these measurements were the first to be reported that included such a large temperature span over the undercooling region. The values that appeared in the literature are summarized in Table I for comparison. Our value agreed with those obtained by Eljutin et al. [19] with the pendant drop and Seydel et al. [20] with the pulse-heating method. It agrees within 2.5% with that measured by Pekarev et al. [21] using the drop technique in vacuum and is

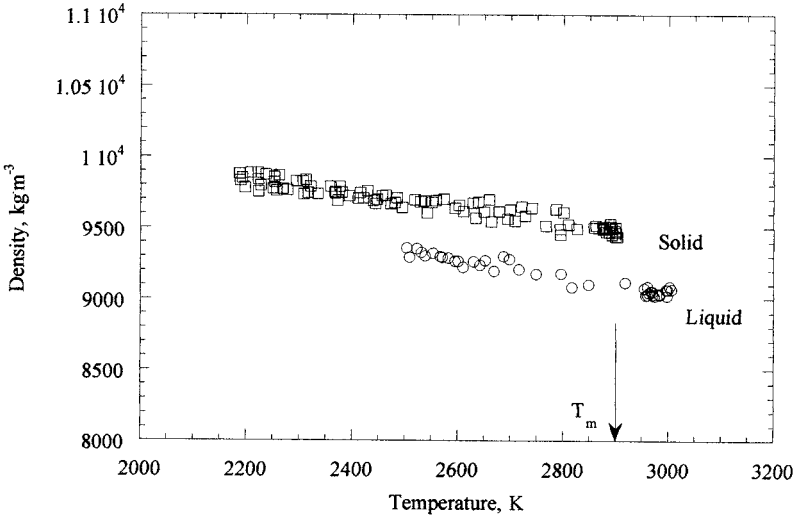

Fig. 4. Density of molybdenum versus temperature.

Table I. Literature Values for the Density of Molybdenum

Density at T_m ($kg \cdot m^{-3}$)	Temperature coeff. (K^{-1})	Temperature (K)	Reference	Technique
9100	−0.60	2,500–3,000	Present work	Levitation
9490[a]	−0.50	2,170–2,890	Present work	Levitation
9100	—	2,896	Eljutin et al. [19]	Pendant drop
9100	—	2,896–7,000	Seydel et al. [20]	Pulse heating
9330	—	2,896	Pekarev [21]	Pendant drop
9350	—	2,896	Allen[22]	Calculation
9350	−0.5	> 2,896	Steinberg [23]	Calculation

[a] Data for the solid phase.

within 2.7% compared with that calculated by Allen [22] from room-temperature specific volumes increased for cubical thermal expansion to the melting point and an estimated value for fusion. Our temperature coefficient was 20% larger than that calculated by Steinberg [23].

The volume variation $V_L(T)$ of the molten state, normalized with the volume at the melting temperature V_m, was derived from Eq. (2) and could be expressed by

$$V_L(T)/V_m = 1 + 6.6 \times 10^{-5}(T - T_m) \qquad (2500 \text{ to } 3000 \text{ K}) \qquad (3)$$

where 6.6×10^{-5} represents the volume expansion coefficient $\alpha_L(T)$. This is, in the first-order approximation, more than 33% smaller than that reported by Seydel et al. [20].

The small discrepancies observed between our results and those of Pekarev et al. [21] and Allen [22] could be attributed to the difference in processing techniques and the extent to which evaporation losses have been considered. We used a containerless approach in vacuum, isolating our samples from container walls and gases, whereas the above authors used methods for which possible chemical reactions between the highly reactive molten molybdenum and residual gases could have altered the final density values.

Figure 4 also illustrates the density measurements for the solid phase over the 2170 to 2890 K temperature range. Again, a linear behavior was observed and the data can be fitted by the following relation:

$$\rho_S(T) = 9.49 \times 10^3 - 0.50(T - T_m) \text{ (kg} \cdot \text{m}^{-3}) \qquad (2170 \text{ to } 2890 \text{ K}) \qquad (4)$$

where T_m is the melting temperature. We believe that these were the first data to be reported for the density of solid molybdenum over such a wide range of high temperatures.

From Eq. (4), the volume variation $V_S(T)$ of the solid phase, normalized with respect to the volume at the melting temperature V_m, can be derived and expressed as

$$V_S(T)/V_m = 1 + 5.3 \times 10^{-5}(T - T_m) \qquad (2170 \text{ to } 2890 \text{ K}) \qquad (5)$$

where 5.3×10^{-5} is the volume expansion coefficient $\alpha_S(T)$.

As shown in Fig. 4, there is a discontinuity in density at the melting temperature, characteristic of a first-order transition. The figure also reveals a convergence between the liquid and the solid trends. The point at convergence may correspond to the undercooling limit before the homogeneous nucleation comes into effect. To investigate this question, further experiments with much smaller samples are planned to further reduce heterogeneous nucleation.

3.2. Constant-Pressure Heat Capacity

The ratio between the constant-pressure heat capacity and the hemispherical total emissivity as a function of the temperature is shown in Fig. 5 for both solid and liquid molybdenum. It is interesting to note that the data for the solid are higher than those for the liquid state. For the liquid

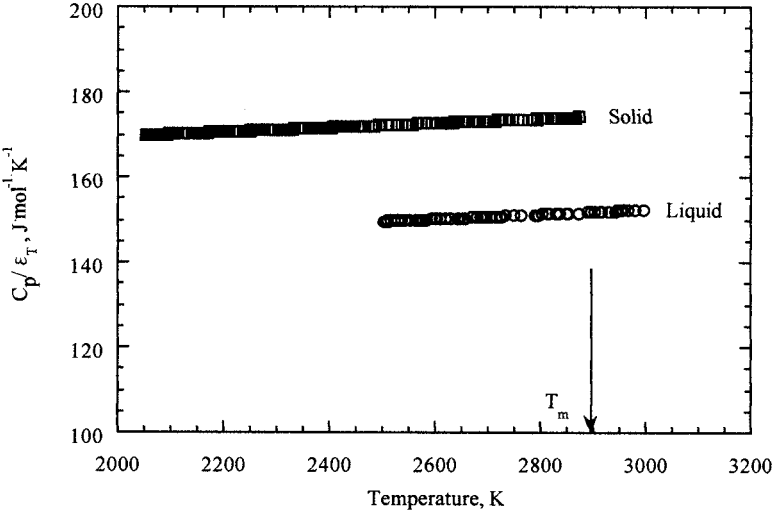

Fig. 5. Ratio between the constant-pressure heat capacity and the hemispherical total emissivity of molybdenum versus temperature.

state, $C_{PL}(T)/\varepsilon_{TL}(T)$ is nearly constant with temperature and can be linearly fitted as

$$C_{PL}(T)/\varepsilon_{TL}(T) = 159.80 + 5.28 \times 10^{-3}(T - T_m)\ (J \cdot mol^{-1} \cdot K^{-1})$$
$$(2500 \text{ to } 3000 \text{ K}) \tag{6}$$

When the value of C_{PL} given by Treverton et al. [24] at the melting temperature was used ($34.23\ J \cdot mol^{-1} \cdot K^{-1}$), ε_{TL} could be determined from Eq. (6) and was equal to 0.21. Although changes in peak emission wavelength with temperature might affect the value of total emissivity as a function of temperature, the lack of data for the overheated and undercooled states of molybdenum prompted us to assume that $\varepsilon_{TL}(T)$ remained constant at a value of 0.21 over the whole temperature range. The temperature dependence of $C_{PL}(T)$ could then be determined from Eq. (6) by simply multiplying it by $\varepsilon_{TL}(T) = 0.21$. The heat capacity so obtained (Fig. 6) could be expressed by the following equation:

$$C_{PL}(T) = 34.2 + 1.13 \times 10^{-3}(T - T_m)\ (J \cdot mol^{-1} \cdot K^{-1}) \qquad (2500 \text{ to } 3000 \text{ K}) \tag{7}$$

At the melting temperature, our value is nearly 40% smaller than that reported by Barin et al. [25]. Figure 5 also shows the ratio between the

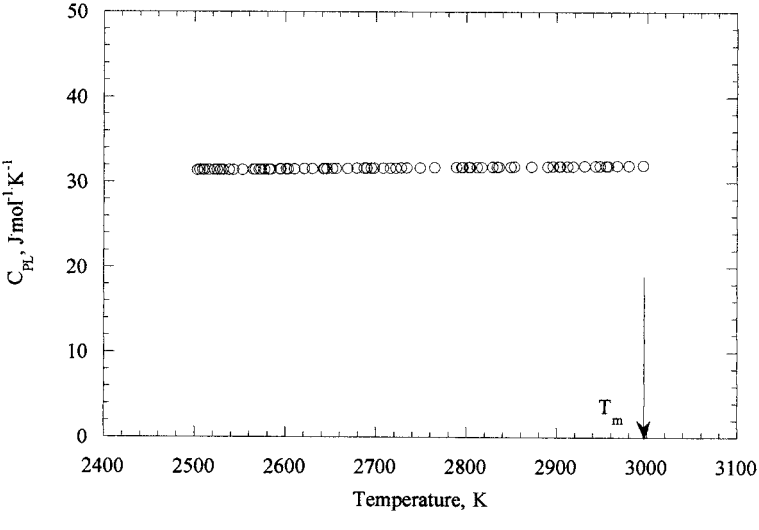

Fig. 6. Heat capacity of liquid molybdenum versus temperature, calculated using the data from Fig. 5 and $\varepsilon_{TL}(T) = 0.21$.

constant-pressure heat capacity and the hemispherical total emissivity as a function of the temperature for solid molybdenum. As for the liquid state, the trend was nearly constant with temperature and could be fitted as

$$C_{PS}(T)/\varepsilon_{TS}(T) = 151.78 + 5.65 \times 10^{-3}(T - T_m)\ (\mathrm{J \cdot mol^{-1} \cdot K^{-1}})$$
$$(2050 \text{ to } 2890\ \mathrm{K}) \tag{8}$$

Similarly, by using the values of $C_{PS}(T)$ given by Cezairliyan et al. [26], it was possible to obtain $\varepsilon_{TS}(T)$, which is expressed as (Fig. 7)

$$\varepsilon_{TS}(T) = 0.29 + 9.86 \times 10^{-5}(T - T_m) \qquad (2050 \text{ to } 2890\ \mathrm{K}) \tag{9}$$

Our value of ε_{TS} at the melting temperature is, within experimental uncertainties, identical to that obtained with an electrical resistivity scheme by Zhorov [27], 9% smaller than that resulting from the pulse-heating technique of Cezairliyan et al. [26], and 14% smaller than that obtained by the tube method of Khrustalev et al. [28]. Our temperature coefficient value is 15% smaller compared to the results given by Zhorov [27], close to 44% higher than that reported by Cezairliyan et al. [26], but slopes in a different direction compared to the value of Khrustalev et al. [28]. We believe that few reasons could explain such discrepancies. Because our sample solidified from a deeply undercooled state, it is possible that its surface

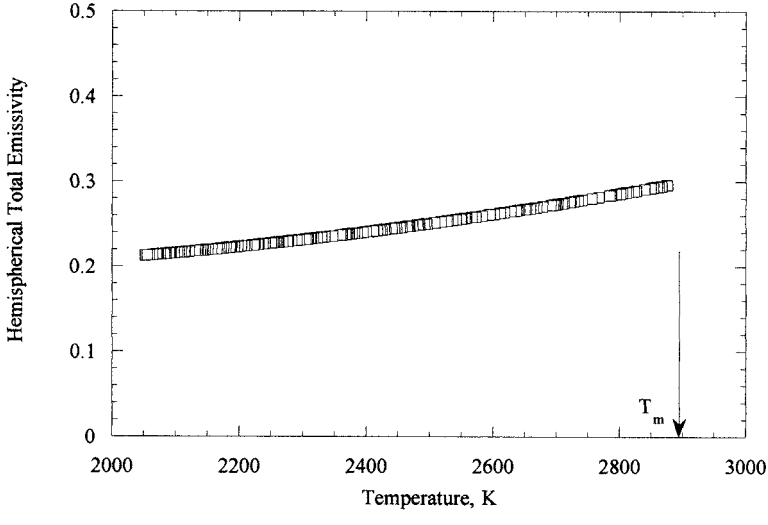

Fig. 7. Hemispherical total emissivity of solid molybdenum versus temperature, calculated using the data from Fig. 5 and $C_{PL}(T)$ from Ref. 26.

Table II. Literature Values for the Latent Heat of Fusion of Molybdenum

Enthalpy of fusion ($J \cdot mol^{-1} \cdot K^{-1}$)	Reference	Method
33.6	Present work	Electrostatic levitation
34.8	Treverton et al. [24]	Drop calorimetry
27.8	Hultgren et al. [28]	Drop calorimetry

structure might be finer than that of other authors, which could have led to a different emissivity value. In addition, the slow reading capability of our pyrometer might have induced a slight shift in the temperature dependence of the emissivity.

In addition, the latent heat of fusion has been determined by adding the enthalpy contributions of the undercooled liquid and that of the isothermal region following the recalescence (see Fig. 3). The contribution of the undercooled portion was found by integrating $C_{PL}(T)$ over temperature from T_m to the lowest temperature of undercooling, whereas that of the isothermal solid was obtained by integrating $\varepsilon_{TS} A\sigma(T^4 - T_{amb}^4)$ over the time at which the solid stays at T_m. The latent heat of fusion was found to be equal to $33.6\ kJ \cdot mol^{-1}$ and compares well with other values found in the literature (Table II). Our value is 3.5% smaller than that given by Treverton et al. [24] and nearly 21% larger than the one given by Hultgren et al. [29], both of which measurements were carried out with a drop calorimeter. Uncertainties in $C_{PL}(T)$ or ε_{TS} might account for the difference. The discrepancy could also be attributed to the slow response of our pyrometer, which lags the recalescence phenomenon, thus inducing errors in time.

4. CONCLUSIONS

We have presented several thermophysical properties of solid and liquid molybdenum measured using the electrostatic levitation furnace developed by NASDA. For the first time, we reported the density of liquid molybdenum over a wide temperature range that included the undercooled state. Also given were the thermal expansion coefficient of both solid and liquid molybdenum and the density of its solid phase over a large temperature span. In addition to the latent heat of fusion, the first results of the ratio of constant-pressure heat capacity to the hemispherical total emissivity of the liquid and solid phases were presented in this paper. Experiments to measure the surface tension and the viscosity of molybdenum are currently under way, and the results will be published soon.

All the thermophysical data presented in this work were obtained from radiative cooling curves and image acquisition. Therefore, to improve our data, efforts should be focused on ways to increase image sharpness, resolution, and contrast. Emphasis should also be directed to devise better numerical techniques to get dT/dt from the cooling curves to diminish numerically induced errors. Current efforts are also devoted to designing a custom-made, fast-response pyrometer to capture more precisely the recalescence phenomenon.

ACKNOWLEDGMENTS

The authors are grateful to Dr. D. W. Bonnell from NIST, who kindly brought the paper by A. Cezairliyan to our attention. Sincere thanks are extended to Dr. J. Yu, Dr. N. Koshikawa, Dr. Y. Arai, Dr. Aoyama, and Dr. Aoki for help at some stage of this work and for challenging discussions.

REFERENCES

1. D. R. Lide and H. P. R. Frederikse (eds.), *CRC Handbook of Chemistry and Physics*, 78th ed. (CRC Press, Boca Raton, FL, 1997).
2. S. Yoda, N. Koshikawa, T. Nakamura, J. Yu, T. Nakamura, Y. Nakamura, S. Yoshitomi, H. Karasawa, T. Ikeda, Y. Arai, M. Kobayashi, Y. Awa, H. Shimoji, T. S. Morita, and S. Shimada, *J. Jpn. Soc. Micrograv. Appl.* **17**:76 (2000).
3. P.-F. Paradis, T. Ishikawa, and S. Yoda, in *Proc. Spacebound 2000* (Vancouver, B.C., Canada, 2000) (in press).
4. P.-F. Paradis, T. Ishikawa, and S. Yoda, in *Proc. First Int. Symp. Micrograv. Res. Appl. Phys. Sci. Biotech.* (Sorrento, Italy, Sept. 2000) (ESA SP-454) (2001), p. 993.
5. T. Ishikawa, P.-F. Paradis, and S. Yoda, *J. Jpn. Soc. Microgrev. Appl.* **17**:98 (2000).
6. T. Ishikawa, P.-F. Paradis, and S. Yoda, *Rev. Sci. Instrum.* **72**:2490 (2001).
7. P.-F. Paradis, T. Ishikawa, and S. Yoda, submitted for publication.
8. P.-F. Paradis, T. Ishikawa, J. Yu, and S. Yoda, *Rev. Sci. Instrum.* **72**:2811 (2001).
9. P.-F. Paradis, T. Ishikawa, and S. Yoda, *J. Mater. Sci.* (in press).
10. W.-K. Rhim, S.-K. Chung, D. Barber, K.-F. Man, G. Gutt, A. A. Rulison, and R. E. Spjut, *Rev. Sci. Instrum.* **64**:2961 (1993).
11. W.-K. Rhim and T. Ishikawa, *Rev. Sci. Instrum.* **69**:3628 (1998).
12. W.-K. Rhim and P.-F. Paradis, *Rev. Sci. Instrum.* **70**:4652 (1999).
13. A. A. Rulison, J. L. Watkins, and B. Zambrano, *Rev. Sci. Instrum.* **68**:2856 (1997).
14. W.-K. Rhim, private communication, *Jet Propulsion Laboratory* (Pasadena, CA, 1998).
15. S.-K. Chung, D. B. Thiessen, and W.-K. Rhim, *Rev. Sci. Instrum.* **67**:3175 (1996).
16. A. A. Rulison and W.-K. Rhim, *Rev. Sci. Instrum.* **65**:695 (1994).
17. W. H. Hofmeister, M. B. Robinson, and R. J. Bayuzick, *Appl. Phys. Lett.* **49**:1343 (1986).
18. D. Turnbull, *J. Appl. Phys.* **21**:1022 (1950).
19. V. P. Eljutin, V. I. Kostikov, and I. A. Penkow, *Poroshk. Met.* **9**:46 (1970).
20. U. Seydel and W. J. Kitzel, *J. Phys. F Metal Phys.* **9**:L153 (1979).
21. V. Pekarev, *Izv. Vys. Uch. Sav. Tsvetn. Met. (USSR)* **6**:111 (1963).
22. B. C. Allen, *Trans. AIME* **227**:1175 (1963).
23. D. J. Steinberg, *Metall. Trans.* **5**:1341 (1974).

24. J. A. Treverton and J. L. Margrave, *Proc. 5th Symp. Thermophys. Props.* (Boston, MA, 1970), pp. 489–494.
25. I. Barin, O. Knacke, and O. Kubaschewski, *Thermodynamic Properties of Inorganic Substances* (Springer Verlag, Berlin, 1977).
26. A. Cezairliyan, M. S. Morse, H. A. Berman, and C. W. Beckett, *J. Res. Natl. Bur. Stand. (U.S.) Phys. Chem.* **74A**:65 (1970).
27. G. A. Zhorov, *High Temp. (USSR)* **5**:881 (1967).
28. B. A. Krustalev, I. P. Kolchenogova, and A. M. Rakov, *High Temp.* **1**:13 (1963).
29. R. Hultgren, R. L. Orr, and K. K. Kelley, *Supplement to Selected Values of Thermodynamic Properties of Alloys and Metals (Metals)* (Lawrence Radiation Laboratory, Berkeley, CA, 1965).